On the Dynamics of Flows Induced by Topographic Ridges

CHANGHENG CHEN AND IGOR KAMENKOVICH

Rosenstiel School of Marine and Atmospheric Science, University of Miami, Miami, Florida

PAVEL BERLOFF

Department of Mathematics, Imperial College London, London, United Kingdom

(Manuscript received 16 July 2014, in final form 28 November 2014)

ABSTRACT

This study describes a nonlocal mechanism for the generation of oceanic alternating jets by topographic ridges. The dynamics of these jets is examined using a baroclinic quasigeostrophic model configured with an isolated meridional ridge. The zonal topographic slopes of the ridge lead to the formation of a system of currents, consisting of mesoscale eddies, meridional currents over the ridge, and multiple zonal jets in the far field. Dynamical analysis shows that transient eddies are vital in sustaining the deep meridional currents over the ridge, which in turn play a key role in the upper-layer potential vorticity (PV) balance. The zonal jets in the rest of the domain owe their existence to the eddy forcing over the ridge but are maintained by the local Reynolds and form stress eddy forcing. The analysis further shows that a broad stable current that either becomes locally nonzonal or encounters a topographic ridge tends to become unstable. This instability provides a vorticity source and generates multiple zonal jets in the far field through a nonlocal mechanism.

1. Introduction

Stationary, multiple zonal jets are clearly visible in planetary atmospheres, with the most well-known example being the banded winds on Jupiter (Kondratyev and Hunt 1982). The detection of the oceanic counterparts of these jets became possible with the advent of long time series of satellite data (Maximenko et al. 2005, 2008). The oceanic jets tend to be quasi stationary and have varying widths and orientations in different parts of the ocean; the jets are also latent, in the sense that they are masked by the surrounding eddies. These peculiarities are in part explained by the presence of the continents, topography, and nonstationary atmospheric forcing in the ocean.

A number of mechanisms of jet formation on the β plane have been proposed. Two-dimensional turbulence theory (Rhines 1975; Vallis and Maltrud 1993; Danilov and Gryanik 2004; Scott and Dritschel 2012) postulates that the flow energy cascades up from short scales until a characteristic meridional scale is eventually reached, at which the effects of Rossby waves channel energy into zonal jets. This scale is called the Rhines scale $L_R = \sqrt{u_{\rm rms}/\beta_0}$, where $u_{\rm rms}$ is the rms velocity of the flow fluctuations, and β_0 is the meridional gradient of the planetary vorticity. The relation of the Rhines scale to the average width of the jets is, however, not universal. Several studies (Panetta 1993; Thompson 2010; Boland et al. 2012) suggested that the width is proportional to L_R, while others (Okuno and Masuda 2003; Maximenko et al. 2005; Berloff 2005; Berloff et al. 2009b) did not.

Jet formation is also described using the zonostrophic theory (Galperin 2004; Galperin et al. 2006), which argues that dynamics of the jets in the oceans and planetary atmospheres are fundamentally the same: both involve the anisotropic inverse energy cascade and exhibit a unique anisotropic energy spectrum. Other mechanisms include the potential vorticity (PV) Phillips effect theory (Baldwin et al. 2007; Dritschel and McIntyre 2008; Wood and McIntyre 2010) and the modulational instability of primary linear waves (Berloff et al. 2009a; Connaughton et al. 2010). These mechanisms are locally controlled in

Corresponding author address: Changheng Chen, Division of MPO, Rosenstiel School of Marine and Atmospheric Science, University of Miami, 4600 Rickenbacker Causeway, Miami, FL 33149.
E-mail: cchen@rsmas.miami.edu

DOI: 10.1175/JPO-D-14-0143.1

the sense that the formation of eddy-driven jets is determined by the properties of the spatially uniform background state or imposed small-scale forcing.

Other mechanisms involve nonlocal mechanisms and nonuniform flows. In particular, the radiating instability of an eastern boundary current can induce zonal jets (Hristova et al. 2008; Wang et al. 2012). Nonlinear interaction between basin modes in a closed ocean basin can also lead to zonal jet formation (Berloff 2005; O'Reilly et al. 2012). Zonal jets can also take the form of β plumes, which are the zonally elongated, gyrelike response to localized vortices' source or sink (Afanasyev et al. 2012; Belmadani et al. 2013; Davis et al. 2014). In particular, Davis et al. (2014) showed that the interaction between the eastern boundary currents with the irregular coastal geometry creates vorticity sources, inducing zonal jets or β plumes in the ocean interior.

Bottom topography is a significant factor in the dynamics of oceanic jets and eddies, and several studies explored the influence of topography on jet properties. By analyzing observations, Sokolov and Rintoul (2007) showed that bottom topography greatly influences the path, width, and intensity of jets in the Southern Ocean. Idealized studies further demonstrated the effects of topography: multiple topographic bumps affect the jet spacing, variability, and meridional transport properties (Thompson 2010); the number of jets varies along a zonally asymmetric ridge (Thompson and Sallée 2012); baroclinic jets are tilted in the presence of a zonal topographic slope and are nearly perpendicular to the barotropic PV gradient (Boland et al. 2012); and eddy kinetic energy is enhanced downstream of isolated topographic features and zonally asymmetric ridges (Witter and Chelton 1998; Thompson and Sallée 2012).

Meridional ridges also can strongly influence the mean circulation. Vallis and Maltrud (1993) found multiple jets along meridional topographic ridges on the f plane and concluded that these jets result from the anisotropic turbulent inverse energy cascade due to the topographic β effect. In an idealized Antarctic Circumpolar Current (ACC) model configured with meridional ridges, Treguier and Panetta (1994) observed two zonal jets with enhanced structure and quasi-stationary meanders leeward of the ridges and found that the jet transport is reduced because of the ridges. MacCready and Rhines (2001) studied the meridional eddy transport in the presence of a meridional ridge and found that the transport increases at and downstream of the ridge. They also observed multiple zonal jets downstream of the ridge but did not explore their dynamics.

In this study, we investigate the mechanism of the formation of quasi-stationary jets in the presence of an isolated meridional ridge. We demonstrate that even a smooth broad ridge can lead to jet formation in an otherwise stable baroclinic flow and that the formation mechanism is fundamentally nonlocal. Previous studies of the formation mechanisms of baroclinic jets focused on either the local baroclinic instability of a strongly sheared flow or the radiating instability of a meridional eastern boundary current. In this study, we propose that a large-scale ridge has far-reaching effects on a zonal flow and can induce zonal jets in the far field by enhancing the baroclinicity and generating vorticity over the ridge region.

This paper is structured in the following way: The model is introduced in section 2. Section 3 demonstrates that a topographic ridge destabilizes an otherwise stable flow and leads to the formation of stationary meridional currents over the ridge, of stationary and migrating zonal jets downstream of the ridge, and of transient eddies in the adjacent regions. Section 4 explores the main dynamical balances, and in section 5, we explore a nonlocal mechanism for the jet formation due to a localized vorticity source. Conclusions are given in section 6.

2. The model

We consider a two-layer quasigeostrophic (QG) model with bottom topography on the β plane (Fig. 1). The PV Q_n in each of the two dynamically active layers is governed by

$$\frac{\partial Q_n}{\partial t} + J(\psi_n, Q_n) = \nu\nabla^4\psi_n - \delta_{n2}\gamma\nabla^2\psi_n, \qquad (1)$$

where the layer index $n = 1, 2$ starts from the top, ψ_n is the streamfunction in the nth layer, $J(,)$ is the Jacobian operator, and δ_{n2} is the Kronecker delta. The terms with ν and γ are the lateral and bottom friction, respectively.

We are interested in the dynamics of a large-scale zonal ocean current with a vertical shear and thus consider a horizontally uniform background flow U in the upper layer and no flow in the deep layer so that

$$\begin{aligned}\psi_1 &= \varphi_1 - Uy,\\ \psi_2 &= \varphi_2,\end{aligned} \qquad (2)$$

where φ_1 and φ_2 describe disturbances around the background flow.

The PV consists of several components, including the relative vorticity of disturbances, the β term, and the stretching terms due to the mean flow, disturbances, and topography:

$$\begin{aligned}Q_n = \nabla^2\varphi_n + [\beta_0 - (-1)^n F_n U]y\\ + (-1)^n F_n(\varphi_1 - \varphi_2) + \delta_{n2} f_0 \frac{\eta_b(x,y)}{H_2},\end{aligned} \qquad (3)$$

where $\beta_0 = 2\times10^{-11}\,\mathrm{m^{-1}\,s^{-1}}$ is the planetary vorticity gradient, H_n are the depths of the layers, $\eta_b(x, y)$ is the

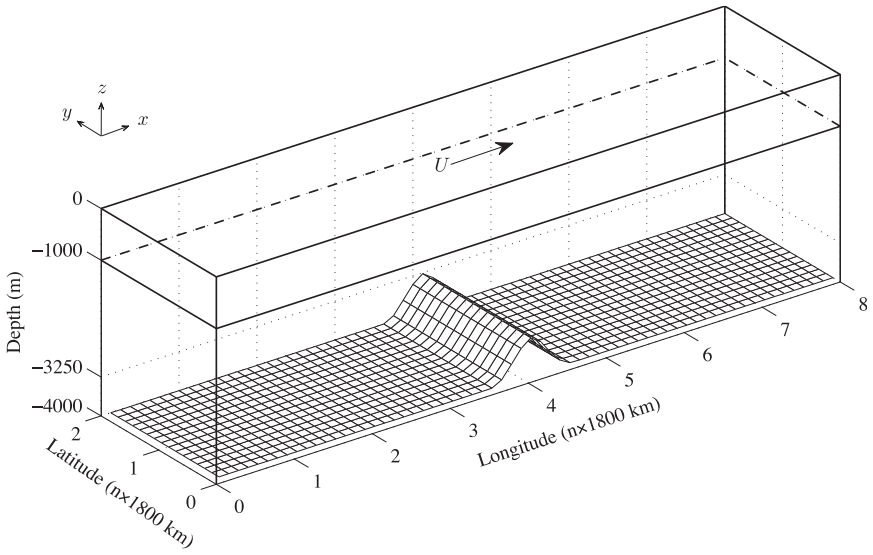

FIG. 1. Sketch of the two-layer model with a topographic ridge at the bottom.

spatially varying elevation of the bottom topography, $F_n = f_0^2/(g'H_n)$ are the stratification parameters, $f_0 = 0.83 \times 10^{-4}\,\mathrm{s}^{-1}$ is the Coriolis parameter, and g' is the reduced-gravity coefficient associated with the density jump between the two layers. We define F as the inverse of the square of the internal Rossby deformation radius $F = f_0^2(H_1 + H_2)/(g'H_1H_2)$ and introduce $\alpha_1 = H_2/(H_1 + H_2)$ and $\alpha_2 = H_1/(H_1 + H_2)$ so that

$$F_1 = \alpha_1 F,$$
$$F_2 = \alpha_2 F. \tag{4}$$

We also introduce a nondimensional parameter

$$S = \frac{f_0 s}{\beta_0 H_2} \tag{5}$$

to characterize the steepness of the bottom topography; s is the slope of the topography.

The computational domain is doubly periodic, with a meridional width of $L_y = 3600\,\mathrm{km}$ and a zonal period of $L_x = 4L_y$. As we will see later, the domain is sufficiently large to fit 26 alternating zonal jets. The grid size is about 7 km. The stratification is defined by $H_1 = 1\,\mathrm{km}$, $H_2 = 3\,\mathrm{km}$, and the internal Rossby deformation radius $F^{-1/2} = 25\,\mathrm{km}$, which is the fundamental length scale for the eddies and jets. The bottom friction is $\gamma = 10^{-7}\,\mathrm{s}^{-1}$, which is close to the value of $1.15 \times 10^{-7}\,\mathrm{s}^{-1}$ used in Arbic and Flierl (2004). Berloff et al. (2011) demonstrated that $\gamma = 10^{-7}\,\mathrm{s}^{-1}$ corresponds to the jets whose relative strength (''latency'') is qualitatively consistent with the observed oceanic jets. The numerical model allows large Reynolds numbers on relatively coarse grids (Karabasov et al. 2009); thus, we use $\nu = 10\,\mathrm{m}^2\,\mathrm{s}^{-1}$. Our convergence tests confirm that the model solutions are nearly the same at increased resolutions.

3. Phenomenology: Jets and eddies

Jet formation in geostrophic turbulence relies on the large-scale PV gradient. In some regions of the ocean, the PV gradient induced by topography can dominate over the planetary PV gradient. The Mid-Atlantic Ridge illustrates this point. The ridge elevation is about 1–3 km, and its width is about 1500 km; therefore, its slopes s can be roughly estimated to be ± 0.7–2.0×10^{-3} on its two sides. In our model, the PV gradient due to the slopes are $f_0 s/H_2 = \pm 2.0$–$5.5 \times 10^{-11}\,\mathrm{m}^{-1}\,\mathrm{s}^{-1}$, which are larger than β_0. Consequently, broad baroclinic currents that are stable over the flat bottom can become unstable over such topographic slopes (Chen and Kamenkovich 2013).

We focus on the effects of meridional ridges. An isolated meridionally uniform ridge (Fig. 1) in this study can be considered an idealized representation of a segment of the Mid-Atlantic Ridge or the Southeast Indian Ridge. Other examples of relevant major topographic features include the Pacific Antarctic Ridge and the Kerguelen Plateau, although the latter feature is more complex. The zonal slopes of the ridge have a strong destabilizing effect on zonal flows, regardless of how weak they are (Chen and Kamenkovich 2013). We illustrate this effect with an eastward background zonal flow $U = 4\,\mathrm{cm\,s}^{-1}$, which is stable over a flat bottom.

The reference solution has a moderately sloped meridional ridge of $s = \pm 10^{-3}$ and $S = \pm 1.4$, which satisfies the constraint of the QG theory that the topographic

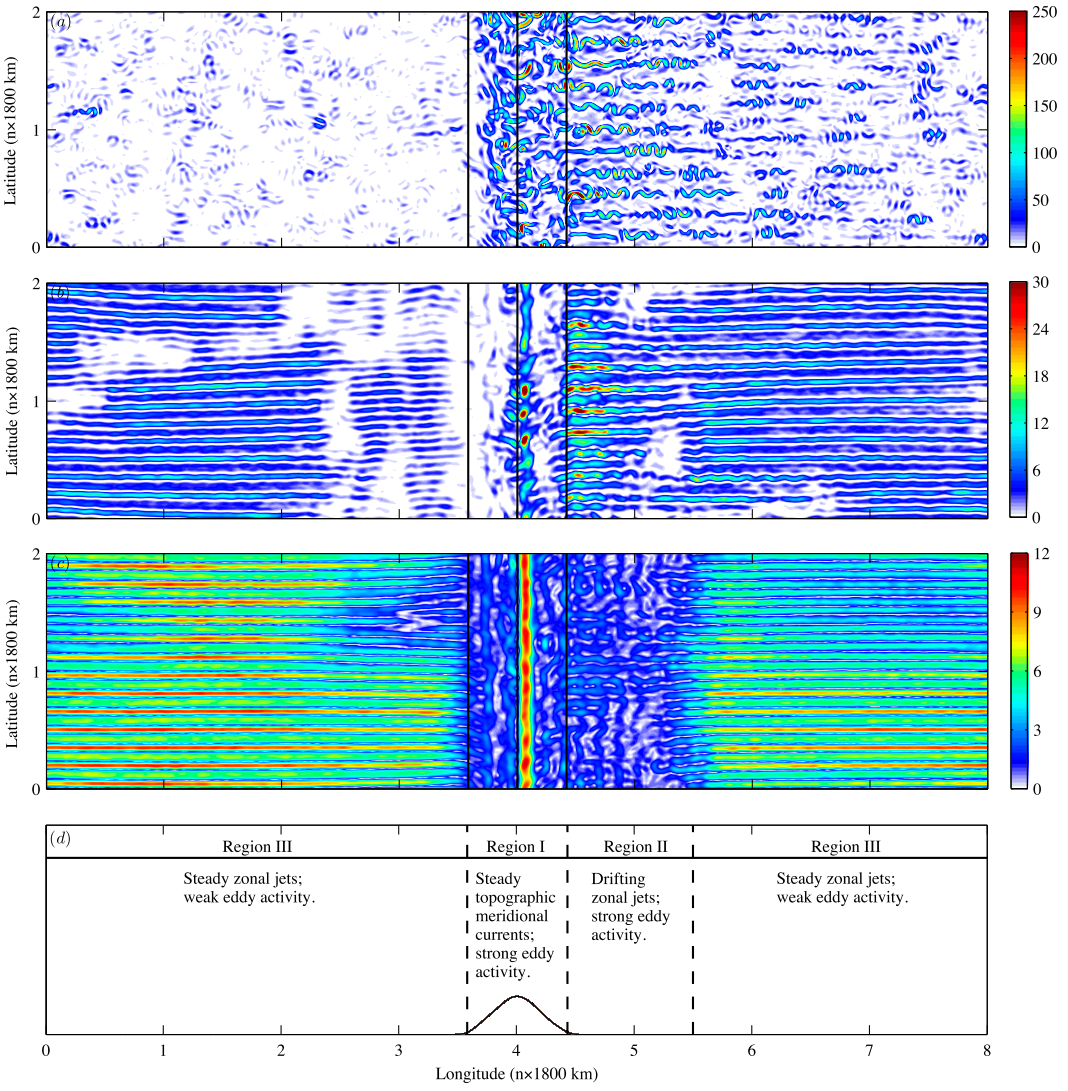

FIG. 2. The system of currents in the model: transient eddies, migrating zonal jets, and stationary meridional and zonal jets. Shown is the kinetic energy ($cm^2\,s^{-2}$) of (a) an instantaneous flow, (b) a 10-yr mean flow, and (c) a 100-yr mean flow in the upper layer of the reference solution. The vertical lines show the position of the ridge. (d) The partition of the domain into three regions based on the flow characteristics. The solid black curve shows the profile of the meridional ridge in the longitude–depth plane.

slope must be much smaller than the flow aspect ratio, which means that $\eta_b/H_2 \ll 1$. The base of the ridge extends 1500 km in longitude, and the height is 750 m at the highest point.

The model is spun up for 5 yr until a statistically steady state is reached. In addition to the constant background flow U in the top layer, the flow has a rich structure consisting of mesoscale eddies, stationary meridional currents on the top of the ridge, migrating quasi-zonal jets, and stationary alternating zonal jets (Fig. 2). Three geographical regions with distinct flow regimes can be identified (Fig. 2): the ridge itself (region I), the area downstream of the ridge with strong transient currents (region II), and the far field with stationary alternating jets (region III). In what follows, we describe the flow properties in these regions.

a. Stationary meridional currents in region I

First, we focus on the flow in region I. As the background flow crosses the ridge, it generates stationary meridional currents over and downstream of the ridge (Figs. 2c, 3). The strongest meridional currents are near the ridge peak: a southward meridional current on the eastern side of the ridge in the deep layer and a northward meridional current above it. We will investigate the dynamical balance of the meridional currents in section 4a.

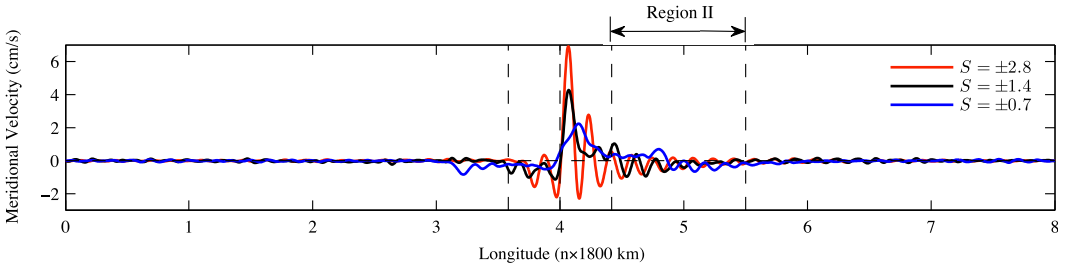

FIG. 3. Meridional currents for three cases with differently sloped meridional ridges. The curves show the meridional average of the time-averaged meridional velocities. The zonal background flow is 4 cm s^{-1} in all the cases.

Adding the background zonal flow U to the upper-layer meridional currents results in a total flow with stationary meanders over and downstream of the ridge. Away from the ridge, the meanders transform into purely zonal motions. In the deep layer, the mean flow follows the ridge. In a QG model configured with a meridional ridge, Abernathey and Cessi (2014) observed similar standing meanders downstream of the ridge, which are responsible for the local heat flux intensification. Such meanders are consistent with the conservation of PV, which demands the creation of anticyclonic circulation due to the squeezing of a water column as it climbs up the ridge. A detailed explanation of the meandering response of eastward flows encountering a meridional ridge is given in Holton (2004).

Characteristics of the topographic meridional currents are closely linked to the steepness of the ridge. We carry out two additional experiments, in which we halve and double the width of the ridge but maintain its height unchanged. Thus, these cases correspond to $S = \pm 2.8$ and $S = \pm 0.7$, respectively. Baroclinic meridional currents are present in both cases, although their properties are different. The currents are more upper-ocean intensified in the case of $S = \pm 2.8$; a similar property was observed in the linear solutions of Chen and Kamenkovich (2013). Over the ridge with $S = \pm 2.8$, the northward meridional current in the upper layer (red line in Fig. 3) is stronger and narrower than the corresponding current over the ridge with $S = \pm 0.7$ (blue line in Fig. 3). In section 4a, we shall see that the surface intensification of the currents is linked to their width and strength through a dynamical balance. Moreover, the meridional currents over the ridge with $S = \pm 0.7$ are less coherent and entail several standing circular loops (Fig. 4a).

The topographic currents remain parallel to the ridge even if the orientation of the ridge on the horizontal plane changes. We rotate the meridional ridge with $S = \pm 1.4$ in the clockwise direction by 30° and 45°. The upper-layer time-averaged flow for the 45° case exhibits topographic currents, which are parallel to the bathymetry (Fig. 4b) and stronger than in the reference solution. The 30° case reveals similar characteristics. In the rest of this paper, only the case with the north–south-oriented and $\pm 10^{-3}$ sloped ridge ($S = \pm 1.4$) will be considered.

b. Jets in regions II and III

Away from the ridge, the flow consists of transient eddies and alternating zonal jets (Fig. 2a). To separate the alternating zonal jets from the transient eddies, we apply a low-pass filter in time (10-yr average), which reveals the jets in regions II and III (Fig. 2b). A very long average over 100 yr does not significantly change the jets in region III but results in very weak circulation in region II. The latter fact indicates that the jets in region II evolve slowly with time.

The width of the jets in regions II and III varies with the eddy energy along the channel, and the jets merge and split accordingly (Fig. 2b). Consistent with the Rhines scaling, the zonal jets are wider in region II since the eddy rms velocity u_{rms} there is larger as well (Fig. 2a). Specifically, the rms velocity in region II is 29% higher than in region III, and the zonal jets in region II are about 14% wider (82 vs 72 km) (Fig. 2b). A transition zone exists between regions II and III, where 22 jets in region II evolve into 26 jets in region III. In particular, four zonal jets split into six jets around $y =$ 900 km (Fig. 2b).

Figure 5 shows the Hovmöller diagram of the time- (10 day) and zonally averaged barotropic zonal velocities in region II. The diagram indicates that the jets migrate southward with a speed of 0.003 cm s^{-1}. Note also that the width of region II is consistent with the zonal decay scale of the meridional currents (Fig. 3). In particular, both the decay scale and the region II width in the cases with $S = \pm 2.8$ and $S = \pm 0.7$ are smaller/larger than those in the reference solution. This suggests that the drift of the jets in region II is tied to the presence of the mean meridional currents. The drift cannot, however, be explained by the meridional advection by the meridional currents over region II since the mean meridional current in region II in the upper layer is about 50 times faster than the southward drift and the lower-layer current is northward.

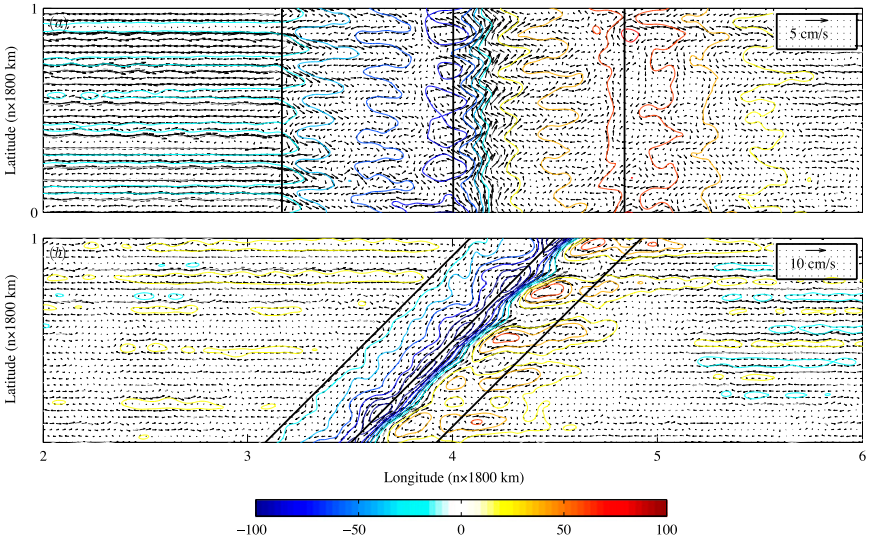

FIG. 4. Time-averaged streamfunction (contours) and velocity (arrows) in the upper layer for the cases of (a) a meridional ridge with $S = \pm 0.7$ and (b) a slanted ridge with $S = \pm 1.4$ and a 45° orientation. The solid lines show the position of the ridges. The zonal background flow is 4 cm s^{-1} in both cases.

Boland et al. (2012) observed drifting jets over topographic slopes and argued that the drift is a consequence of PV conservation. However, the drift that we observe occurs downstream of the meridional ridge, and it is over the flat bottom. In section 4b, we will further explore the dynamical reasons behind this drift.

4. The importance of eddies in the jet dynamics

In this study, eddies have an impact on the mean flow by redistributing PV. We study this impact here through the eddy PV flux convergence ("eddy forcing"), which can be viewed as an internally generated forcing of the mean flow. In the baroclinic system, this eddy forcing comprises convergences of the Reynolds and form stresses.

a. *The role of eddies in the dynamical balance of the meridional currents*

First, we focus on the role of eddies in the dynamical balance of the stationary meridional currents. To do so, we take the time average of the QG equations and obtain

$$\overline{J(\varphi_1, q_1)} + U\overline{q_{1x}} + (\beta_0 + F_1 U)\overline{\varphi_{1x}} = \nu\nabla^4\overline{\varphi_1}, \quad \text{and} \qquad (6)$$

$$\overline{J(\varphi_2, q_2)} + (\beta_0 - F_2 U)\overline{\varphi_{2x}} - f_0\frac{\eta_{b_x}}{H_2}\overline{\varphi_{2y}} = \nu\nabla^4\overline{\varphi_2} + \gamma\nabla^2\overline{\varphi_2}, \qquad (7)$$

where $q_1 = \nabla^2\varphi_1 - F_1(\varphi_1 - \varphi_2)$, $q_2 = \nabla^2\varphi_2 + F_2(\varphi_1 - \varphi_2)$, and the overbars indicate the time averages. We further separate the flow into the time-averaged and eddying components: $\varphi_n = \overline{\varphi_n} + \varphi_n'$, where $\overline{\varphi_n}$ stands for the time-averaged streamfunction, and φ_n' is the residual perturbation streamfunction describing the transient eddies.

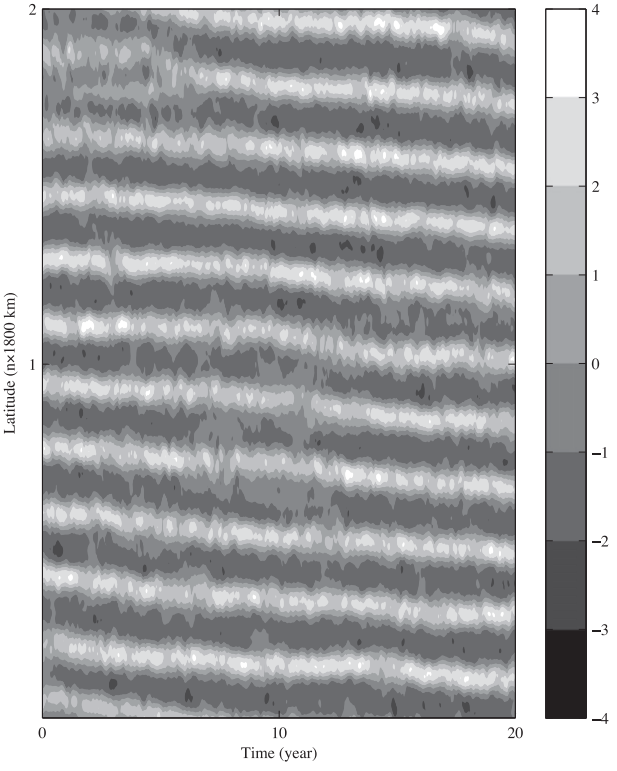

FIG. 5. Drift of the jets as shown by the time series of zonal averages of 10-day mean, barotropic zonal velocities (cm s^{-1}) in region II. The jets drift southward with a speed of 0.003 cm s^{-1}.

An examination of each of the terms in the above equations leads to the following balances over region I, within 1% accuracy. In the upper layer, there is a linear balance between the advection of the PV of the meridional currents by U and the advection of the planetary vorticity by $\overline{v_1}$:

$$U\overline{v_{1xx}} + UF_1\overline{v_2} + \beta_0\overline{v_1} = 0. \tag{8}$$

In the deep layer, the advection term $\overline{J(\varphi_2, q_2)} = J(\overline{\varphi_2}, \overline{q_2}) + \overline{J(\varphi_2', q_2')}$ is dominated by the eddy forcing component (second term). The stationary flow over the ridge is predominantly meridional; hence, $J(\overline{\varphi_2}, \overline{q_2})$ is negligible, and, to the leading order, we have a balance between $\overline{J(\varphi_2', q_2')}$ and the meridional advection of the background PV by $\overline{v_2}$:

$$\overline{J(\varphi_2', q_2')} + (\beta_0 - F_2U)\overline{v_2} = 0. \tag{9}$$

The topographic terms do not enter the balance explicitly, and their role is in destabilizing the flow and generating the eddy forcing. The essential role of the eddy forcing is consistent with Holloway (1992), who showed that, in a barotropic flow, the eddy forcing over a meridional ridge supports the formation of a topographic mean flow via the so-called Neptune effect. Here, we observe that in a baroclinic flow, the deep topographic currents play a key role in maintaining the upper-layer meridional currents via tilting the layer interface.

The entire meridional currents have a strong baroclinic component. This baroclinicity is further outlined by the strong negative correlation between $\overline{v_1}$ and $\overline{v_2}$ of -0.84. This high correlation enables us to find an analytical solution of Eq. (8) by assuming that $\overline{v_2} = \alpha\overline{v_1}$ ($\alpha < 0$ is a constant):

$$U\overline{v_{1xx}} + (\beta_0 + \alpha UF_1)\overline{v_1} = 0, \tag{10}$$

and the solution is

$$\overline{v_1}(x) = \begin{cases} C_1 \cos\left[\left(\dfrac{\beta_0 + \alpha UF_1}{U}\right)^{1/2} x\right] + C_2 \sin\left[\left(\dfrac{\beta_0 + \alpha UF_1}{U}\right)^{1/2} x\right], & \alpha > -\dfrac{\beta_0}{UF_1}, \\ C_1 \exp\left[\left(-\dfrac{\beta_0 + \alpha UF_1}{U}\right)^{1/2} x\right] + C_2 \exp\left[-\left(-\dfrac{\beta_0 + \alpha UF_1}{U}\right)^{1/2} x\right], & \alpha < -\dfrac{\beta_0}{UF_1}, \end{cases} \tag{11}$$

where C_1 and C_2 are constants. Equation (11) helps to interpret the numerical solutions. First, the meridional structure of the solution depends on the parameter α, and a large negative α corresponds to a single meridional jet trapped to the ridge crest [the second solution in Eq. (11)]. In contrast, our reference solution has $\alpha \approx -0.21$, which is larger than $-\beta_0/UF_1 \approx -0.42$. Thus, the first analytical solution in Eq. (11) is relevant, and there are alternating meridional currents that are not trapped to the ridge. Second, the eddy forcing in the deep layer has a strong influence on the structure of these jets. In particular, if $\overline{v_2} = 0$ (or $\alpha = 0$) because of a hypothetical absence of eddy forcing in the deep layer, $\overline{v_1}$ would have very narrow alternating currents.

b. The role of eddies in maintaining the zonal jets

In this section, the nonlinear dynamics of the zonal jets will be illuminated by the analysis of the role of eddy forcing in supporting the jets in regions II and III.

In region III, the leading-order time-averaged PV balance is between the Reynolds stress forcing (RSF), form stress forcing (FSF), dissipation (Diss), and bottom friction (Fric):

$$\overline{J(\varphi_n', \nabla^2\varphi_n')} + \overline{J[\varphi_n', (-1)^n F_n(\varphi_1' - \varphi_2')]} = \nu\nabla^4\overline{\varphi_n} - \delta_{n2}\gamma\nabla^2\overline{\varphi_n}, \tag{12}$$

where the left-hand side terms are the two components of the total eddy forcing (TEF), and the terms on the right-hand side are the dissipation and bottom friction associated with the zonal jets. Berloff et al. (2009b) also observed such a balance for the zonal jets in a QG model with a flat bottom. The Reynolds stress can be interpreted as an effective turbulent viscosity and can be a source or sink of large-scale PV. The form stress here represents the transfer of the zonal momentum between the two layers, and it is proportional to the meridional flux of the density.

We examine the roles of the different terms in Eq. (12) by studying their correlations with the PV anomalies associated with the jets. A positive (negative) correlation of the terms with the PV anomalies means that they support (resist) the jets. Table 1 shows the correlation coefficients of the zonally averaged PV anomalies with the zonally averaged terms in Eq. (12). The dissipation and bottom friction always tend to resist the jets as indicated by the positive correlation coefficients. In the upper layer, the RSF supports, while the FSF resists, the jets. These relationships are further

TABLE 1. Correlation coefficients of the zonal jet PV with the Diss, Fric, RSF, FSF, and TEF.

	Region II					Region III				
	Diss	Fric	RSF	FSF	TEF	Diss	Fric	RSF	FSF	TEF
Upper layer	0.75	—	−0.83	0.80	0.13	0.63	—	−0.99	0.98	−0.94
Deep layer	0.83	0.99	−0.67	−0.56	−0.61	0.65	0.86	−0.92	−0.99	−1.00

illustrated in Figs. 6a–d, which show the zonally averaged terms overlaid on the zonally averaged PV anomalies in the upper layer in region III. In the deep layer, both the RSF and FSF support the zonal jets (figure not shown).

In region II, the zonal jets are quasi stationary and do not follow the PV balance of Eq. (12). As indicated by the positive correlation coefficients in Table 1, both the dissipation and bottom friction tend to resist the jets. In the upper layer, the RSF supports the jets and the FSF resists the jets; these relationships are further shown in Figs. 7b and 7c. In the deep layer, both the RSF and FSF support the jets as they do in region III (figure not shown).

The total eddy forcing, the sum of RSF and FSF, plays different roles in regions II and III. The TEF coincides almost perfectly with the PV anomalies in region III (Fig. 6e); in contrast, the TEF in region II is shifted southward relative to the PV anomalies (Fig. 7e). This is further indicated by the low correlation coefficient of 0.13 between the two terms in region II in contrast to 0.94 in region III. The off-core eddy forcing on the zonal jets in region II acts to push the jets southward, resulting in the meridional drift of the jets. Both components of the total eddy forcing are important in this regard.

The origins of this eddy-induced drift are not entirely clear. A study of barotropic jets excited by prescribed forcing (K. Srinivasan, UCLA, 2014, personal communication) suggests that jet drift is a universal consequence of the breaking reflection symmetry by spatial structure of eddy forcing, and the jets will drift if the phase lines of the eddy forcing are not parallel or perpendicular to the lines of the background PV. We hypothesize that the formation of meridional currents downstream of the ridge causes nonzonal orientation of the mean PV contours, which renders asymmetries in the eddy forcing and results in the jet drift.

5. A nonlocal mechanism for jet formation

Although the zonal jets are maintained by the local eddy forcing, as shown in the last section, we conclude that the zonal jets owe their existence to the localized vorticity source over the ridge through a nonlocal mechanism. In this section, we discuss the results that support this conclusion.

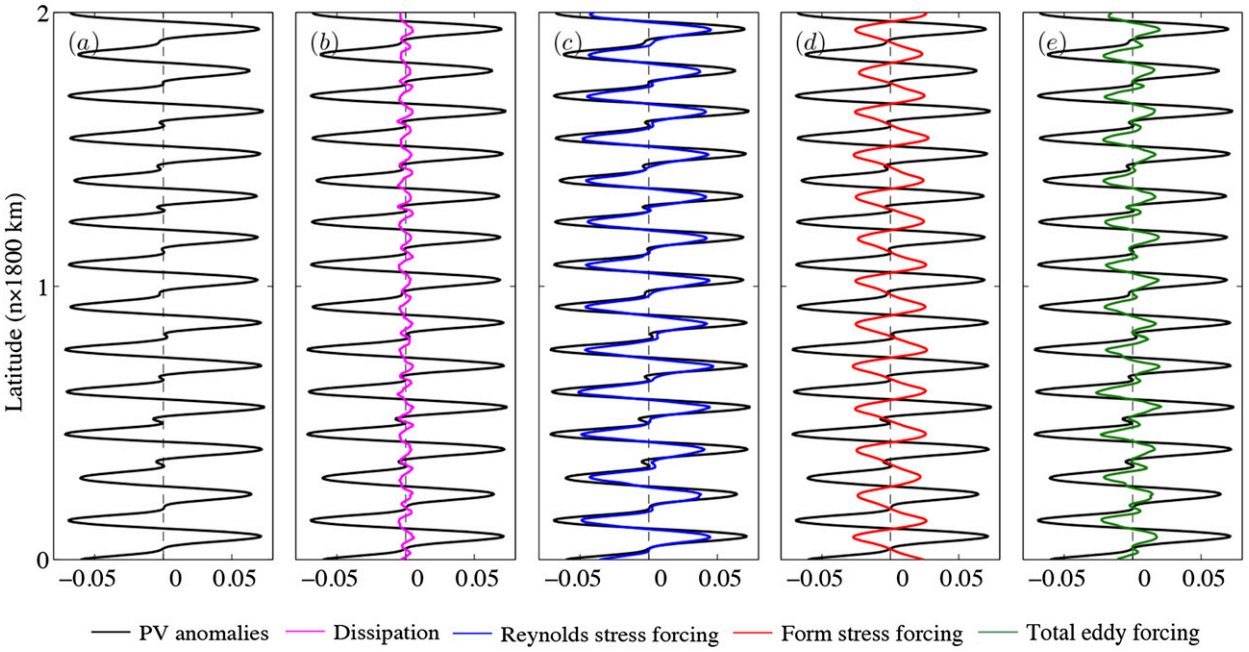

FIG. 6. Eddy forcing (s^{-2}) in region III in the upper layer. Zonal averages of 10-yr mean (b) dissipation, (c) Reynolds stress forcing, (d) form stress forcing, and (e) total eddy forcing overlaid on (a) the PV anomalies associated with the zonal jets.

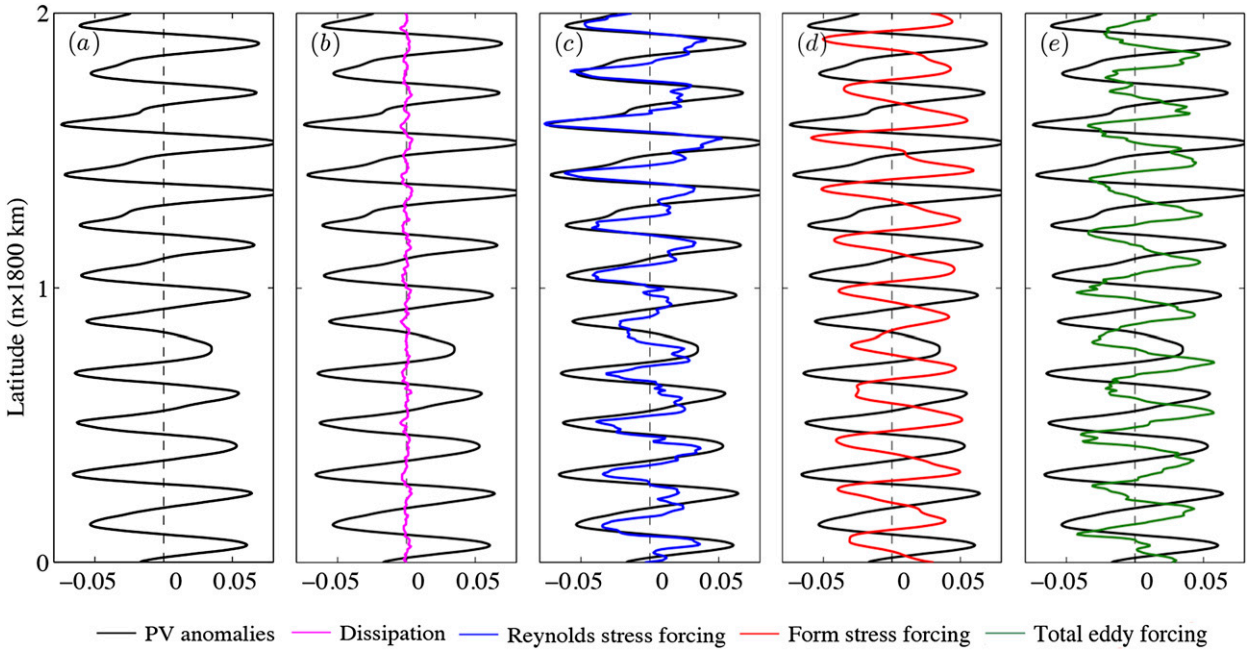

FIG. 7. As in Fig. 6, but for region II.

Vorticity anomalies originate from the local baroclinic instability over the ridge and propagate eastward. This can be seen from Fig. 8a, which shows a 10-yr mean distribution of enstrophy defined here as the square of relative PV. The values are the largest over and downstream of the ridge, indicating the existence of a vorticity source over this region. To examine the propagation of the vorticity anomalies, we plot the Hovmöller diagram of the enstrophy over 5 yr in Fig. 8b. This figure shows intense vorticity generation events over the ridge and the subsequent vorticity anomalies propagating eastward with a speed of approximately $1\,\mathrm{cm\,s^{-1}}$. This eastward propagation and subsequent decay of vorticity anomalies would not, however, result in time-mean zonal jets unless these anomalies are concentrated along some preferred latitudes.

A comparison between the spatial structure of the enstrophy in Fig. 8a with that of the zonal jets in Fig. 2b reveals an important property—not only do the vorticity anomalies tend to stay on certain latitudes, but the enstrophy tends to concentrate on the eastward jets. This is in contrast to the low levels of enstrophy along the westward zonal jets. Berloff and Kamenkovich (2013) also demonstrated that some of the coherent vortices preferentially straddle eastward jets.

To demonstrate that the zonal jets arise from nonlocal vorticity sources, we design three experiments using the same model but with a flat bottom. The first experiment (Expt1) is configured with the localized eddy forcing from the reference solution; the second one (Expt2) is configured with a localized stochastic eddy forcing; and the third one (Expt3) has a locally nonzonal background flow. We will see that all these simulations exhibit multiple zonal jets. We remind the reader that the background zonal flow would be stable and the jet formation would not be possible in the absence of these vorticity sources or the meridional component of the background flow.

a. *Can the eddy forcing over the ridge induce zonal jets?*

The first experiment examines the role of the deep eddy forcing over the ridge in generating zonal jets in the far field. For this purpose, we replace the ridge with a flat bottom and introduce a PV source into region I in the deep layer. The PV equations become

$$\frac{\partial Q_n}{\partial t} + J(\psi_n, Q_n) = \delta_{n2}\mathcal{F}_n + \nu\nabla^4\psi_n - \delta_{n2}\gamma\nabla^2\psi_n, \qquad (13)$$

where Q_n is given by Eq. (3) without the topographic term, and $\mathcal{F}_n$ is the eddy source, which equals the time-averaged eddy forcing over region I from our reference solution (Fig. 9a). Despite the importance of this eddy forcing in maintaining the meridional currents in the reference solution, introducing it into the model with a flat bottom does not lead to the formation of meridional currents. Instead, new eddies are formed, and they act to cancel the PV source locally in the time-mean sense. This implies that the formation of the meridional currents relies on the topographic β effect due to the

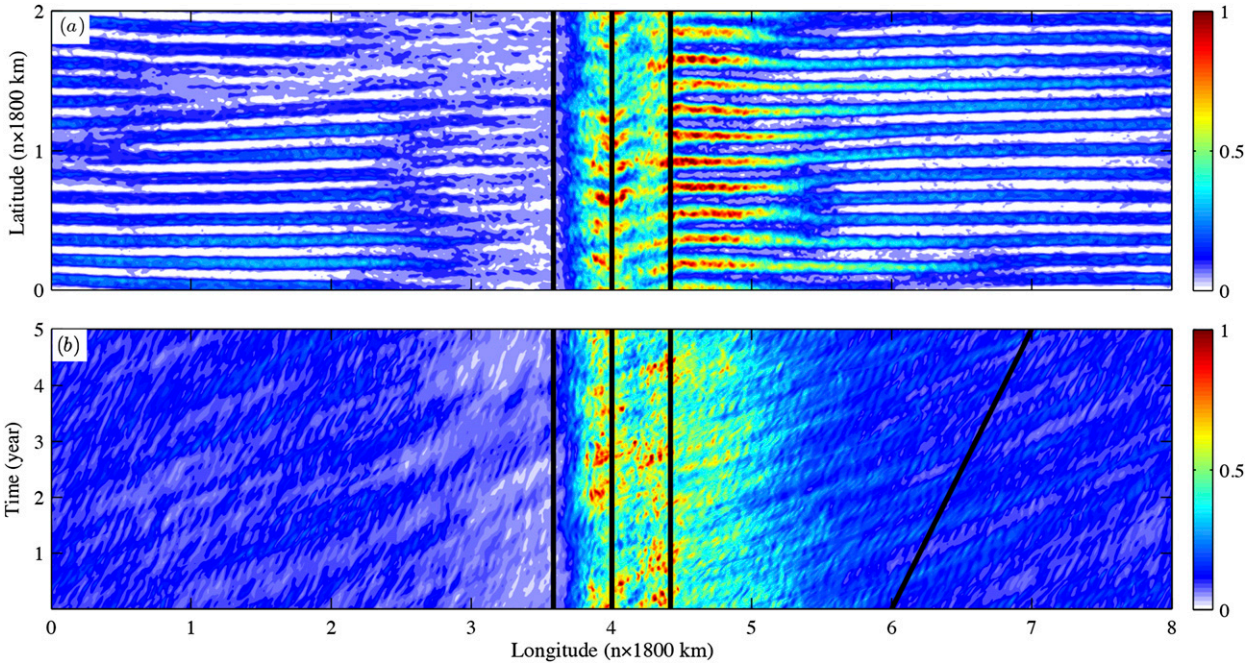

FIG. 8. Enstrophy (s^{-2}) for the reference solution. (a) A 10-yr mean of the enstrophy. (b) The Hovmöller diagram of the meridionally averaged enstrophy. The enstrophy propagates eastward at a speed of about 1 cm s^{-1}. The vertical lines show the position of the ridge, and the angled black line indicates the propagation in the space–time plane.

meridional ridge, consistent with the conjecture of the Neptune effect.

The deep-layer eddy forcing generates alternating zonal jets in the far field, confirming the key role of the ridge-induced vorticity source in the jet dynamics. These zonal jets (Figs. 9b,c) closely resemble those in our reference solution. In particular, as in the reference solution, the zonal jets downstream of the eddy forcing region are stronger and wider than those in the far field; consequently, the zonal jets undergo splitting and merging events. These properties are consistent with the Rhines scaling.

b. *Zonal jet formation due to a localized stochastic forcing*

Is the exact spatial structure of the vorticity source ($\delta_{n2}\mathscr{F}_n$ used in Expt1) important for the jet formation? To answer this question, we carried out the second experiment with a localized stochastic forcing in the deep layer in region I. The stochastic forcing is white in time, and its spatial correlations are below the grid resolution. The strength of the stochastic forcing is comparable to that of the eddy forcing in Expt1.

Multiple alternating zonal jets form in the far field (figure not shown), demonstrating that a localized vorticity source can effectively generate zonal jets, but its spatial structure is not critical for the jet formation. The jets in this experiment are similar to those in Expt1. One distinction is that they are wider than those in Expt1: 16 jets form in the channel in Expt2 in contrast to 26 in Expt1.

The characteristics of the zonal jets, however, depend on the strength of the stochastic forcing. In a separate experiment, we choose a stochastic forcing whose strength is 10 times weaker and observe noticeable changes in the properties of the corresponding zonal jets. In particular, 26 jets form in the domain, which are less latent and narrower than those from Expt2. A detailed investigation of the dependence of the zonal jets on the strength of the stochastic forcing is beyond the scope of this study. Berloff (2005) observed jet formation due to a homogeneous stochastic forcing; our results show that a localized stochastic forcing can induce jets in the far field.

c. *Zonal jet formation in a locally nonzonal background flow*

The third experiment studies the formation of zonal jets by a localized vorticity source due to a locally nonzonal background flow over a flat bottom. This locally nonzonal flow is inherently unstable (Kamenkovich and Pedlosky 1994) and can support unstable modes of two types: those that grow fast and are trapped to the ridge and those that are slowly growing but have a long oscillating tail (''radiating modes'') (Kamenkovich and Pedlosky 1996; Hristova et al. 2008). The first type of unstable modes will effectively correspond to a vorticity source, similar to those in Expt1 and Expt2; the second type can

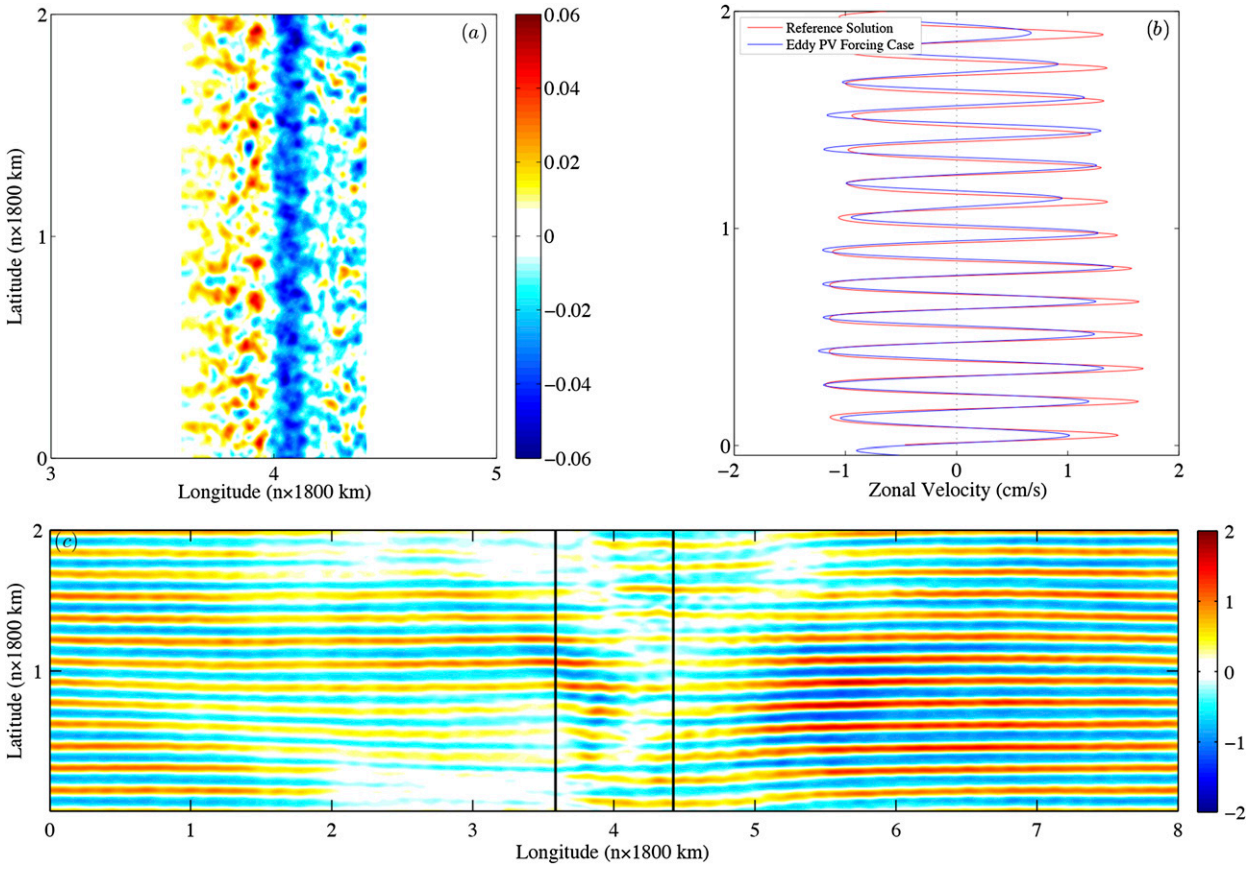

FIG. 9. Zonal jets induced by the localized eddy forcing from the reference solution. (a) The eddy forcing $\overline{J(\varphi_2', q_2')}$ in the deep layer over the ridge region (s^{-2}). (b) Time- and zonally averaged barotropic zonal velocity from Expt1 (blue curve) overlaid on its counterpart from the reference solution (red curve). (c) Time-averaged barotropic zonal velocity from Expt1. The solid lines denote the forcing region.

participate in triad interactions with the trapped modes and render zonal jets (Wang et al. 2012).

We impose a locally nonzonal flow in the upper layer—the mean flow is purely zonal and has a velocity of U everywhere, except over the region where it is nonzonal with (U, V) velocities. The governing PV equations become

$$\frac{\partial q_1}{\partial t} + J(\varphi_1, q_1) + (\beta_0 + F_1 U)\frac{\partial \varphi_1}{\partial x} - \frac{\partial Z}{\partial x}\frac{\partial \varphi_1}{\partial y} + U\frac{\partial q_1}{\partial x} + V\frac{\partial q_1}{\partial y} = \nu\nabla^4\varphi_1 + \mathcal{F}^*, \quad \text{and} \tag{14}$$

$$\frac{\partial q_2}{\partial t} + J(\varphi_2, q_2) + (\beta_0 - F_2 U)\frac{\partial \varphi_2}{\partial x} = \nu\nabla^4\varphi_2 - \gamma\nabla^2\varphi_2, \tag{15}$$

where V is the meridional flow in the upper layer, $Z = (\partial V/\partial x) - F_1 \int V\,dx$ is the PV gradient associated with the meridional flow, and

$$\mathcal{F}^* = -(\beta_0 + F_1 U)V_1 - U\partial Z/\partial x + \nu\nabla^4\left(\int V\,dx\right) \tag{16}$$

is the additional forcing term required to maintain the meridional flow.

We choose a subcritical background zonal flow $U = 4\,\mathrm{cm\,s^{-1}}$, and a meridional flow

$$V(x) = A\,\mathrm{sech}^2\left(\frac{x - C}{W}\right), \tag{17}$$

where A is the magnitude of the meridional flow, C determines the position of its peak, and W defines its width. We set $A = 4\,\mathrm{cm\,s^{-1}}$ and choose $W = 100\,\mathrm{km}$ (solid line in Fig. 10b).

The system reaches a statistical equilibrium characterized by baroclinic meridional currents near the region of the mean flow nonzonality (Fig. 10b) and by alternating zonal jets in the rest of the domain (Fig. 10a). Secondary meridional currents emerge in both layers as a result of the rectification of the flow (Fig. 10b), but the resulting mean flow remains nonzonal in the unstable region. Zonal jets downstream of the unstable region are stronger than those over the rest of the channel, and, unlike the jets in region II of the reference solution, they

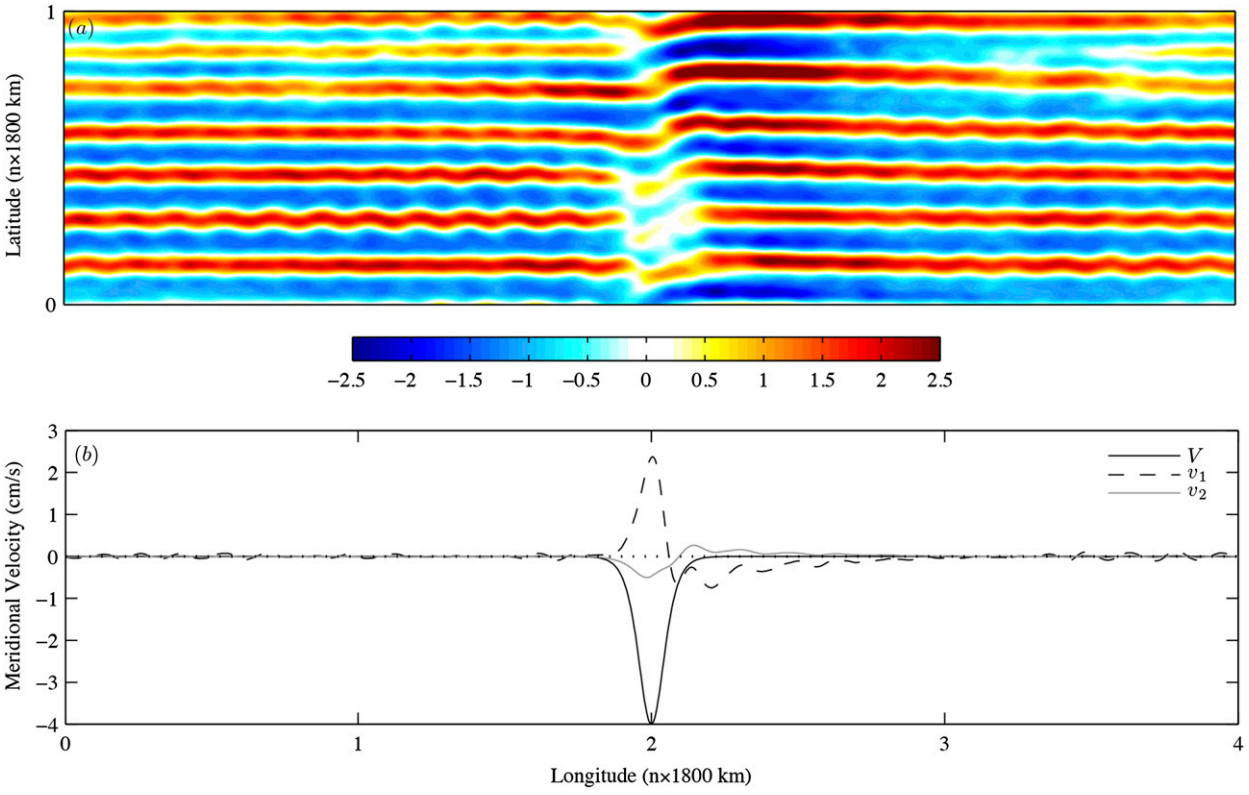

FIG. 10. Solution with a locally nonzonal background flow and a flat bottom. (a) A 20-yr mean of the barotropic zonal velocity of the zonal jets. (b) The background meridional flow V and the corresponding 20-yr mean meridional velocities $\overline{v}_1$ and $\overline{v}_2$.

do not drift meridionally. Also, the positions of the zonal jets upstream and downstream of the unstable region are shifted; thus, the zonal jets are slightly slanted but continuous across the periodic channel. In addition, alternating zonal jets also form in the same model if V is replaced with the strongest baroclinic meridional current taken from the reference solution.

6. Summary and conclusions

In this study, we identify and explore a mechanism of the generation of multiple zonal jets by an isolated, meridionally uniform topographic ridge. The zonal slopes of this ridge destabilize an otherwise stable eastward background flow, as in the linear study by Chen and Kamenkovich (2013), and this instability leads to the formation of a nonlinear system of currents, consisting of mesoscale eddies, stationary meridional currents over the ridge, migrating zonal jets downstream of the ridge, and stationary alternating zonal jets in the far field. Eddy forcing is essential for the dynamics of these currents. In particular, multiple zonal jets emerge in response to an eddy-induced PV source in the ridge vicinity. The generated vorticity anomalies propagate eastward, along preferred zonal pathways, and the corresponding eddy forcing acts to sustain the stationary jets in the far field. In addition to this remote influence, eddies over the ridge induce baroclinic meridional currents, as is demonstrated by the baroclinic PV balance, and this is consistent with the Neptune effect first discussed by Holloway (1992) for a barotropic system.

The eddy generation over the ridge serves as a vorticity source for the eddies and eddy-driven zonal jets in the flat bottom part of the domain. These zonal jets cannot form unless such a vorticity source is present. This is demonstrated by three numerical simulations, in which the meridional ridge is replaced with a flat bottom, and a localized eddy forcing or a locally nonzonal background flow is introduced. The presence of the local vorticity source related to the region of enhanced instability seems to be a fundamental element of the nonlocal mechanism of jet generation in all the three cases. Propagating vorticity anomalies would not, however, lead to the jet formation if they were not concentrated along some preferred latitudes. This self-organization of the eddies seem to be a fundamental property of the geostrophic turbulence on the β plane, as has also been reported in other geophysical flows.

Another nonlocal mechanism of jet generation involves the nonlinear interactions of nontrapped (“radiating”) and localized unstable modes (Wang et al. 2012). Although it is

challenging to isolate the importance of this radiating instability mechanism in our study, this mechanism can potentially be active in our simulation with a locally nonzonal background flow. The similarity of the jet properties in this numerical experiment to those in other simulations, however, suggests a smaller importance of the radiating instability in this study.

Another interesting aspect of the flow near the ridge is the meridional drift in zonal jets, also observed by Thompson (2010) over a range of simple topography and by Boland et al. (2012) in the case of a uniform zonal and meridional slope. We demonstrate that the drift is a result of the eddy forcing being out of phase with the positions of the zonal jets at the lee of the ridge. The fundamental reason for this effect remains unclear. K. Srinivasan and W. R. Young (2014, unpublished manuscript) demonstrate that the drifting jets always result if the phase lines of the eddy forcing are not parallel or perpendicular to the mean PV contours. It is, therefore, plausible that the formation of the meridional currents over and downstream of the ridge renders nonzonal PV contours and induces asymmetries in the spatial structure of the eddy forcing, leading to the jet drift.

The nonlocal mechanism of this study is likely to be important in the real ocean. The ubiquitous oceanic jets owe their existence, at least partly, to the surrounding nonzonal topographic ridges. Realistic topographic features, more complex than those considered in this study, include small-scale ridges and troughs. These additional jet-scale features can directly induce zonal jets through the β-plume mechanism. Our study, however, demonstrates that this small-scale forcing is not required for the jet formation and that a large-scale meridional ridge can effectively render eddy-driven jets. Our study also suggests that the jets drift and merge/split downstream of the ridge and that stationary jets should exist only far away from topographic features. This property may render the existence of stationary jets nearly impossible. However, the essential elements of jet formation over a flat bottom, such as the importance of secondary instabilities and eddy forcing, are likely to be universal even in realistic complex configurations. Future study of jet formation over complex topographic features requires more advanced models with continuous stratification and configured with realistic topography. It would also be interesting to explore the dynamics of topographic currents by analyzing satellite data and comprehensive numerical simulations.

Acknowledgments. We thank William Johns, Tamay Özgökmen, and two anonymous reviewers for their helpful advice on improving this manuscript. This study was supported by the National Science Foundation, Grants OCE-0842834 and OCE-1154923.

REFERENCES

Abernathey, R., and P. Cessi, 2014: Topographic enhancement of eddy efficiency in baroclinic equilibration. *J. Phys. Oceanogr.,* **44,** 2107–2126, doi:10.1175/JPO-D-14-0014.1.

Afanasyev, Y. D., S. O'Leary, P. B. Rhines, and E. Lindahl, 2012: On the origin of jets in the ocean. *Geophys. Astrophys. Fluid Dyn.,* **106,** 113–137, doi:10.1080/03091929.2011.562896.

Arbic, B. K., and G. R. Flierl, 2004: Effects of mean flow direction on energy, isotropy, and coherence of baroclinically unstable beta-plane geostrophic turbulence. *J. Phys. Oceanogr.,* **34,** 77–93, doi:10.1175/1520-0485(2004)034<0077:EOMFDO>2.0.CO;2.

Baldwin, M. P., P. B. Rhines, H.-P. Huang, and M. E. McIntyre, 2007: The jet-stream conundrum. *Science,* **315,** 467–468, doi:10.1126/science.1131375.

Belmadani, A., N. A. Maximenko, J. P. Mccreary, R. Furue, O. V. Melnichenko, N. Schneider, and E. D. Lorenzo, 2013: Linear wind-forced beta plumes with application to the Hawaiian Lee Countercurrent. *J. Phys. Oceanogr.,* **43,** 2071–2094, doi:10.1175/JPO-D-12-0194.1.

Berloff, P., 2005: On rectification of randomly forced flows. *J. Mar. Res.,* **63,** 497–527, doi:10.1357/0022240054307894.

——, and I. Kamenkovich, 2013: On spectral analysis of mesoscale eddies. Part II: Nonlinear analysis. *J. Phys. Oceanogr.,* **43,** 2528–2544, doi:10.1175/JPO-D-12-0233.1.

——, ——, and J. Pedlosky, 2009a: A mechanism of formation of multiple zonal jets in the oceans. *J. Fluid Mech.,* **628,** 395–425, doi:10.1017/S0022112009006375.

——, ——, and ——, 2009b: A model of multiple zonal jets in the oceans: Dynamical and kinematical analysis. *J. Phys. Oceanogr.,* **39,** 2711–2734, doi:10.1175/2009JPO4093.1.

——, S. Karabasov, J. T. Farrar, and I. Kamenkovich, 2011: On latency of multiple zonal jets in the oceans. *J. Fluid Mech.,* **686,** 534–567, doi:10.1017/jfm.2011.345.

Boland, E. J. D., A. F. Thompson, E. Shuckburgh, and P. H. Haynes, 2012: The formation of nonzonal jets over sloped topography. *J. Phys. Oceanogr.,* **42,** 1635–1651, doi:10.1175/JPO-D-11-0152.1.

Chen, C., and I. Kamenkovich, 2013: Effects of topography on baroclinic instability. *J. Phys. Oceanogr.,* **43,** 790–804, doi:10.1175/JPO-D-12-0145.1.

Connaughton, C. P., B. T. Nadiga, S. V. Nazarenko, and B. E. Quinn, 2010: Modulational instability of Rossby and drift waves and generation of zonal jets. *J. Fluid Mech.,* **654,** 207–231, doi:10.1017/S0022112010000510.

Danilov, S., and V. M. Gryanik, 2004: Barotropic beta-plane turbulence in a regime with strong zonal jets revisited. *J. Atmos. Sci.,* **61,** 2283–2295, doi:10.1175/1520-0469(2004)061<2283:BBTIAR>2.0.CO;2.

Davis, A., E. Di Lorenzo, H. Luo, A. Belmadani, N. Maximenko, O. Melnichenko, and N. Schneider, 2014: Mechanisms for the emergence of ocean striations in the North Pacific. *Geophys. Res. Lett.,* **41,** 948–953, doi:10.1002/2013GL057956.

Dritschel, D. G., and M. E. McIntyre, 2008: Multiple jets as PV staircases: The Phillips effect and the resilience of eddy-transport barriers. *J. Atmos. Sci.,* **65,** 855–874, doi:10.1175/2007JAS2227.1.

Galperin, B., 2004: The ubiquitous zonal jets in the atmospheres of giant planets and Earth's oceans. *Geophys. Res. Lett.,* **31,** L13303, doi:10.1029/2004GL019691.

——, S. Sukoriansky, N. Dikovskaya, P. L. Read, Y. H. Yamazaki, and R. Wordsworth, 2006: Anisotropic turbulence and zonal jets in rotating flows with a β-effect. *Nonlinear Processes Geophys.,* **13,** 83–98, doi:10.5194/npg-13-83-2006.

Holloway, G., 1992: Representing topographic stress for large-scale ocean models. *J. Phys. Oceanogr.,* **22,** 1033–1046, doi:10.1175/1520-0485(1992)022<1033:RTSFLS>2.0.CO;2.

Holton, J. R., 2004: *An Introduction to Dynamic Meteorology.* 4th ed. Academic Press, 535 pp.

Hristova, H. G., J. Pedlosky, and M. A. Spall, 2008: Radiating instability of a meridional boundary current. *J. Phys. Oceanogr.,* **38,** 2294–2307, doi:10.1175/2008JPO3853.1.

Kamenkovich, I. V., and J. Pedlosky, 1994: Instability of baroclinic currents that are locally nonzonal. *J. Atmos. Sci.,* **51,** 2418–2433, doi:10.1175/1520-0469(1994)051<2418:IOBCTA>2.0.CO;2.

——, and ——, 1996: Radiating instability of nonzonal ocean currents. *J. Phys. Oceanogr.,* **26,** 622–643, doi:10.1175/1520-0485(1996)026<0622:RIONOC>2.0.CO;2.

Karabasov, S. A., P. S. Berloff, and V. M. Goloviznin, 2009: CABARET in the ocean gyres. *Ocean Modell.,* **30,** 155–168, doi:10.1016/j.ocemod.2009.06.009.

Kondratyev, K., and G. Hunt, 1982: *Weather and Climate on Planets.* Elsevier, 768 pp.

MacCready, P., and P. B. Rhines, 2001: Meridional transport across a zonal channel: Topographic localization. *J. Phys. Oceanogr.,* **31,** 1427–1439, doi:10.1175/1520-0485(2001)031<1427:MTAAZC>2.0.CO;2.

Maximenko, N. A., B. Bang, and H. Sasaki, 2005: Observational evidence of alternating zonal jets in the World Ocean. *Geophys. Res. Lett.,* **32,** L12607, doi:10.1029/2005GL022728.

——, O. V. Melnichenko, P. P. Niiler, and H. Sasaki, 2008: Stationary mesoscale jet-like features in the ocean. *Geophys. Res. Lett.,* **35,** L08603, doi:10.1029/2008GL033267.

Okuno, A., and A. Masuda, 2003: Effect of horizontal divergence on the geostrophic turbulence on a beta-plane: Suppression of the Rhines effect. *Phys. Fluids,* **15,** 56–65, doi:10.1063/1.1524188.

O'Reilly, C. H., A. Czaja, and J. H. LaCasce, 2012: The emergence of zonal ocean jets under large-scale stochastic wind forcing. *Geophys. Res. Lett.,* **39,** L11606, doi:10.1029/2012GL051684.

Panetta, R. L., 1993: Zonal jets in wide baroclinically unstable regions: Persistence and scale selection. *J. Atmos. Sci.,* **50,** 2073–2106, doi:10.1175/1520-0469(1993)050<2073:ZJIWBU>2.0.CO;2.

Rhines, P. B., 1975: Waves and turbulence on a beta-plane. *J. Fluid Mech.,* **69,** 417–443, doi:10.1017/S0022112075001504.

Scott, R. K., and D. G. Dritschel, 2012: The structure of zonal jets in geostrophic turbulence. *J. Fluid Mech.,* **711,** 576–598, doi:10.1017/jfm.2012.410.

Sokolov, S., and S. R. Rintoul, 2007: Multiple jets of the Antarctic Circumpolar Current south of Australia. *J. Phys. Oceanogr.,* **37,** 1394–1412, doi:10.1175/JPO3111.1.

Thompson, A. F., 2010: Jet formation and evolution in baroclinic turbulence with simple topography. *J. Phys. Oceanogr.,* **40,** 257–278, doi:10.1175/2009JPO4218.1.

——, and J.-B. Sallée, 2012: Jets and topography: Jet transitions and the impact on transport in the Antarctic Circumpolar Current. *J. Phys. Oceanogr.,* **42,** 956–972, doi:10.1175/JPO-D-11-0135.1.

Treguier, A. M., and R. L. Panetta, 1994: Multiple zonal jets in a quasigeostrophic model of the Antarctic Circumpolar Current. *J. Phys. Oceanogr.,* **24,** 2263–2277, doi:10.1175/1520-0485(1994)024<2263:MZJIAQ>2.0.CO;2.

Vallis, G. K., and M. E. Maltrud, 1993: Generation of mean flows and jets on a beta plane and over topography. *J. Phys. Oceanogr.,* **23,** 1346–1362, doi:10.1175/1520-0485(1993)023<1346:GOMFAJ>2.0.CO;2.

Wang, J., M. A. Spall, G. R. Flierl, and P. Malanotte-Rizzoli, 2012: A new mechanism for the generation of quasi-zonal jets in the ocean. *Geophys. Res. Lett.,* **39,** L10601, doi:10.1029/2012GL051861.

Witter, D. L., and D. B. Chelton, 1998: Eddy–mean flow interaction in zonal oceanic jet flow along zonal ridge topography. *J. Phys. Oceanogr.,* **28,** 2019–2039, doi:10.1175/1520-0485(1998)028<2019:EMFIIZ>2.0.CO;2.

Wood, R. B., and M. E. McIntyre, 2010: A general theorem on angular-momentum changes due to potential vorticity mixing and on potential-energy changes due to buoyancy mixing. *J. Atmos. Sci.,* **67,** 1261–1274, doi:10.1175/2009JAS3293.1.